THE JOURNAL OF PHYSICAL CHEMISTRY C

Article

Cite This: J. Phys. Chem. C 2018, 122, 2122−2126

pubs.acs.org/JPCC

Wetting Transition of a Cylindrical Cavity Engraved on a Hydrophobic Surface

Hyojeong Kim,[†,§,⊥] Man Yeong Ha,[‡] and Joonkyung Jang*[,†]

[†]Department of Nanoenergy Engineering and [‡]School of Mechanical Engineering, Pusan National University, Busan 46241, Republic of Korea

[§]Max-Planck-Institut für Intelligente Systeme, Heisenbergstrasse 3, Stuttgart 70569, Germany

[⊥]Institut für Theoretische Physik IV, Universität Stuttgart, Pfaffenwaldring 57, Stuttgart 70569, Germany

Supporting Information

ABSTRACT: This study theoretically examines the wetting of a cylindrical cavity engraved on a hydrophobic surface, in the context of the Cassie−Baxter-to-Wenzel transition of a water drop resting on such a surface. The stable, metastable, and transition states and their free energies are identified by constructing the free-energy profile of the wetting process. Wetting starts with a liquid−vapor interface pinned at the top edge of the cavity and proceeds with a symmetrically depinned interface. The liquid−vapor interface later becomes annular upon its touching of the bottom of the cavity and finally asymmetric before the cavity is fully wetted by the liquid. This study examines the effects of the cavity geometry and the pressure of the liquid on the wetting and dewetting transitions.

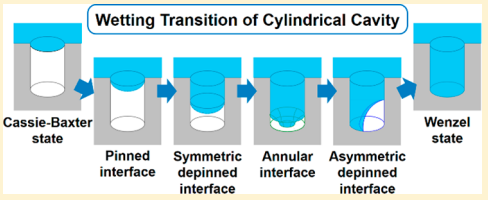

INTRODUCTION

Superhydrophobic surfaces are used in numerous applications, including water harvesting,[1] impermeable textiles,[2] antifogging,[3] and self-cleaning paint.[4] Inspired by natural surfaces, such as lotus leaves and rose petals, a superhydrophobic surface is typically constructed by engraving a regular array of micro- or nanoscale cavities. Periodic cylindrical holes[5,6] and rectangular trenches[7,8] are commonly engraved for this purpose.

A macroscopic water drop resting on top of such small scale cavities can wet or dewet the underlying cavities, giving rise to so-called the Wenzel[9] (WZ) or Cassie−Baxter[10] (CB) state of the drop, respectively. Because the transition of a water drop to the WZ state deteriorates the hydrophobicity of a surface, a cavity that gives rise to a stable CB state (which decreases the contact area of the drop and the surface) is desirable. If a stable CB state is not feasible, a long-lived metastable CB state is preferred instead. In any case, a cavity that gives rise to a high free-energy barrier for its wetting (CB to WZ) is suitable for superhydrophobic applications.[11,12]

Understanding the stable, metastable, and transition states in wetting and the free-energy barriers between these states can provide a design principle for a cavity to be engraved on a superhydrophobic surface. From a scientific viewpoint, the wetting or dewetting transition of a confined system is a fundamental problem pertaining to a range of phenomena in various disciplines. Giacomello et al.[13] presented a theory for the wetting of a two-dimensional rectangular trench by constructing the free-energy profile for the wetting. Herein, this paper presents a theory for the wetting of a cylindrical cavity, which is a common motif for cavities engraved on superhydrophobic surfaces. The intermediate and metastable states and their free energies in the wetting of cylindrical cavities are uncovered. By solving the liquid−vapor interface either analytically or numerically, a cylindrical cavity is shown to be wetted in four steps. The liquid−vapor interface is first pinned symmetrically and then depinned. With further wetting, the interface becomes annular upon touching the bottom of the cavity and finally asymmetric. The free-energy barrier for the wetting or dewetting transition is investigated by varying the aspect ratio of the cavity and the pressure of the wetting liquid.

THEORY

Consider a cylindrical cavity with a width W and a depth D (as shown in Figure 1). A macroscopic water drop much larger than the cavity is resting on top of the cavity ($z > D$). The CB-to-WZ transition of the drop can be regarded as the wetting transition of the cavity.[14,15] The grand potential of the fluid inside the cavity, Ω,[13] relative to that of the fully wetted cavity (the WZ state) can be expressed

$$\Omega = \Delta P V_v + \gamma_{lv} A_{lv} + \gamma_{lv} A_{sv} \cos\theta \quad (1)$$

where V_v is the vapor volume inside the cavity, A_{lv} and A_{sv} are the areas of the liquid−vapor and solid−vapor interfaces, respectively, γ_{lv} is the liquid−vapor-interfacial tension, and θ is the *intrinsic* contact angle of the water drop on a flat surface. ΔP is the pressure of the liquid in excess of the vapor pressure. By design, Ω is 0 for the fully wetted WZ state. In addition, Ω is subject to a constraint, $X = \chi V_{cavity}$, where χ ($\chi \leq 1$) is the dimensionless filling level of the cavity, and V_{cavity} is the volume of the cavity.

Received: October 2, 2017
Revised: January 14, 2018
Published: January 17, 2018

DOI: 10.1021/acs.jpcc.7b09757
J. Phys. Chem. C 2018, 122, 2122−2126

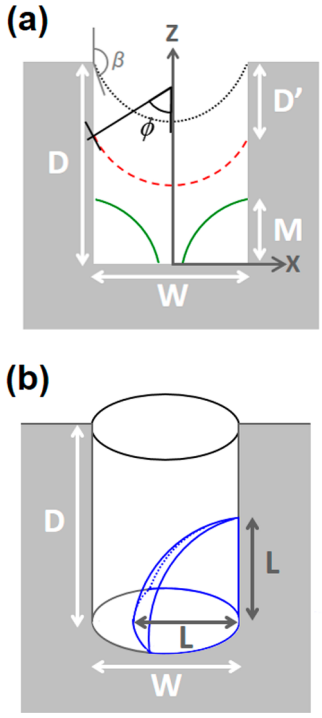

Figure 1. Various liquid−vapor interfaces in the wetting of a cylindrical cavity. D and W refer to the depth and width of the cavity, respectively. (a) Axis-symmetric interfaces of liquid and vapor. Shown is the cross section of the cavity taken along the XZ plane where the Z axis is the symmetry axis. The pinned, depinned, and annular interfaces are drawn as dotted, broken, and solid lines, respectively. β is the angle between the liquid−vapor and solid−liquid interfaces. φ is the angle between the vector normal to the liquid−vapor interface and the symmetry axis. D' represents the depth of the symmetric depinned interface. The annular interface intersects the bottom and side of the cavity at a distance, M, from the bottom corner of the cavity. (b) Asymmetric depinned interface of liquid and vapor. This interface intersects the bottom and side of the cavity at a distance, L, from the bottom corner of the cavity.

Consequently, the grand potential to be minimized is $\Omega - \lambda(V_l - X)$, where λ is a Lagrange multiplier, and V_l is the liquid volume inside the cavity.

To calculate Ω, it is important to determine the liquid−vapor interface, $z(x)$, where z is the height measured from the bottom of the cavity, and x ($|x| \le W/2$) is the lateral position measured from the symmetry axis (Figure 1a). By writing $\Omega - \lambda(V_l - X)$ as $\int f(z, \dot{z}, x)\, dx$, where $\dot{z} = dz/dx$, then

$$f(z, \dot{z}, x) = 2\pi\left[\Delta P z x + \gamma_{lv} x\sqrt{\dot{z}^2 + 1} + \gamma_{lv}\cos\theta\,(x + D) - \lambda(D - z - \chi D)x\right] \tag{2}$$

The Euler−Lagrange equation, $-\frac{d}{dx}\left[\frac{\partial f}{\partial \dot{z}}\right] + \frac{\partial f}{\partial z} = 0$, is then given by a modified Young−Laplace equation,

$$\Delta P + \lambda = \gamma_{lv}\left[\frac{\ddot{z}}{(1 + \dot{z}^2)^{3/2}} + \frac{\dot{z}}{x\sqrt{1 + \dot{z}^2}}\right] = \gamma_{lv}\kappa \tag{3}$$

where κ is the mean curvature of the liquid−vapor interface. The same equation was obtained by Giacomello et al.[13] using a different variational approach. The derivation of eqs 2 and 3 are detailed in the Supporting Information.

To solve eq 3, we introduce a new variable, $u = -\sin\phi$,[16,17] where ϕ is the angle made by the vector normal to the liquid−vapor interface and the symmetry axis of the cavity (Figure 1a). Equation 3 is written as a differential equation of u, which is solved either analytically or numerically. For the case of a rectangular groove, the exact solutions of eq 3 can be derived for all three types of liquid−vapor interfaces studied by Giacomello et al.:[13] a symmetric pinned interface, a symmetric depinned interface, and an asymmetric depinned interface (see the Supporting Information, Figure S1 and eqs S4−S6).

In the present case of a cylindrical cavity, the liquid−vapor interface takes four different shapes. Initially, the interface is pinned symmetrically at the top edge of the cavity and then becomes depinned symmetrically (Figure 1a). The interface afterward becomes annular upon touching the bottom of the cavity, and finally remains asymmetric until the cavity is fully wetted by the liquid (Figure 1b). The symmetric pinned interface is expressed exactly by

$$z = D + \frac{W}{2\cos\beta}\left[\sqrt{1 - \left(\frac{2\cos\beta}{W}x\right)^2} - \sin\beta\right], \quad \left(0 \le x \le \frac{W}{2}\right) \tag{4}$$

where β is the angle between the liquid−vapor and solid−liquid interfaces (see Figure 1a). β follows Gibbs' criterion,[18] $\theta - \pi/2 \le \beta \le \theta$, depending on the filling level, χ. The symmetric depinned interface is given by an analytic function,

$$z = D - D' + \frac{W}{2\cos\theta}\left[\sqrt{1 - \left(\frac{2\cos\theta}{W}x\right)^2} - \sin\theta\right] \tag{5}$$

where D' is the depth of the triple line, which is the contact line of the liquid−vapor interface with the solid wall of the cavity (Figure 1a).

A new type of liquid−vapor interface is also discovered: an annular interface, which is drawn as the solid lines in Figure 1a. Here, the symmetric depinned interface touches the bottom of the cavity and flips its downward curvature to an upward one. The liquid−vapor interface $z(x)$ can be written as

$$z = -\frac{1}{k}\left(\sqrt{1 - \frac{k^2}{4x^2}\left(\frac{W^2}{4} + \frac{W}{k}\cos\theta - x^2\right)^2} + \cos\theta\right) + \frac{|k|}{k^2}\left\{-\frac{1}{A}[E(\varphi, A) - E(\varphi_0, A)] + \frac{(1 - A^2)}{A}[F(\varphi, A) - F(\varphi_0, A)]\right\} \tag{6}$$

where $k = \frac{W\cos\theta + 2M\sin\theta}{M^2 - W^2/4}$, and M is the distance of the triple line from the bottom corner of the cavity (Figure 1a). $F(\varphi, A)$ and $E(\varphi, A)$ are the incomplete elliptic integrals of first and second kind: $F(\varphi, A) = \int_0^{\varphi} \frac{1}{\sqrt{1 - A^2\sin^2\alpha}}\, d\alpha$ and $E(\varphi, A) = \int_0^{\varphi} \sqrt{1 - A^2\sin^2\alpha}\, d\alpha$, where $A = \frac{2}{\sqrt{k^2W^2 + 4kW\cos\theta + 4}}$, $\varphi_0 = \frac{\pi}{2} - \theta$, $\theta - \frac{\pi}{2} \le \varphi \le \pi - \theta$. The details for derivation of eqs 4−6 are provided in the Supporting Information.

DOI: 10.1021/acs.jpcc.7b09757
J. Phys. Chem. C 2018, 122, 2122−2126

The asymmetric interface of the liquid and vapor are calculated numerically. Briefly, a sphere with a radius R_S, whose center lies outside the cavity (which lies in the XZ plane of Figure 1b), is set up. The surface of the sphere intersects the bottom and side of the cavity at a distance L from the bottom corner of the cavity. The overlapping regions of the sphere and cavity are taken to be in the vapor phase. By inspection of the geometry,[13] R_S can be expressed in terms of L and θ as $R_S = \frac{L}{\sin\theta + \cos\theta}$. L is adjusted so that the vapor volume and contact angle match the desired values $(1-\chi)V_{cavity}$ and θ, respectively.

Using the liquid–vapor interfaces given by eqs 4–6, the corresponding grand potentials, Ωs, are obtained. The Ω of the symmetric pinned interface is given by

$$\Omega = \frac{1}{4}\pi W^2 \Delta P\left[D - \frac{1}{2}W\tan\beta - \frac{1}{3}W\left(\tan^3\beta - \frac{1}{\cos^3\beta}\right)\right] - \frac{1}{2}\pi W\gamma_{lv}\left[W\left(\frac{\tan\beta}{\cos\beta} - \frac{1}{\cos^2\beta}\right) - 2\cos\theta\left(\frac{1}{4}W + D\right)\right] \quad (7)$$

In the case of a symmetric depinned interface,

$$\Omega = \frac{1}{4}\pi W^2 \Delta P\left[D - D' - \frac{1}{2}W\tan\theta - \frac{1}{3}W\left(\tan^3\theta - \frac{1}{\cos^3\theta}\right)\right] - \frac{1}{2}\pi W\gamma_{lv}\left[W\left(\frac{\tan\theta}{\cos\theta} - \frac{1}{\cos^2\theta}\right) - 2\cos\theta\left(\frac{1}{4}W + D - D'\right)\right] \quad (8)$$

Equations 7 and 8 are also derived in detail in the Supporting Information. The Ω of the annular interface is calculated by evaluating the vapor volume, V_v, and the interfacial areas, A_{lv} and A_{sv}. Suppose the triple lines are at a distance M from the bottom corners of the cavity (Figure 1a). V_v is then given by $V_v = \int_M^{W/2} 2\pi z x \, dx$, where $z(x)$ is given by eq 6. This integral is evaluated numerically. A_{lv} is given by $A_{lv} = \int_M^{W/2} 2\pi x\sqrt{\dot{z}^2 + 1}\, dx$, which is calculated by numerical integration. A_{sv} is simply given by $A_{sv} = \pi(W^2/4 - M^2) + \pi WM$. The Ω of the asymmetric depinned interface is calculated following a similar numerical procedure. For comparison, the Ωs for the liquid–vapor interfaces found in the wetting of a rectangular groove are also shown in the Supporting Information (eqs S7–S9).

Throughout this work, the pressure, ΔP, is reported as a dimensionless pressure, ΔP^*, defined as $\Delta P^* = \Delta P/\Delta P_{max}$, where $\Delta P_{max} = -4\gamma_{lv}\cos\theta/W$. ΔP_{max} is the pressure above which the wetting transition experiences no free-energy barrier (the case where $\lambda = 0$ in eq 3). ΔP_{max} was also derived by Patankar[19] using a different formalism. In a typical experiment, $W = 1$ μm, $\alpha = D/W = 1$, and $\theta = 110°$. Using $\gamma_{lv} = 0.0721$ N/m, $\Delta P_{max} = 0.9735$ atm is found for this case. Ω is also reported as a dimensionless quantity, Ω*, defined as $\Omega^* = \Omega/\Omega_{max}$, where $\Omega_{max} = \Delta P_{max} V_{cavity}$. For a typical microscale cavity ($D = W = 1$ μm), $\Omega_{max} = \Delta P_{max} V_{cavity} = 7.75 \times 10^{-14}$ J $= 1.87 \times 10^7 \, k_B T$.

RESULTS AND DISCUSSION

The free-energy profile of the wetting transition is examined by varying the pressure as $\Delta P^* = 0.01$, 0.7, and 1. In Figure 2, Ω* is plotted by varying the filling level, χ, from −0.2 to 1 (a negative χ indicates an upward curvature of the pinned interface). The contact angle, θ, is set to a typical experimental value of 110°.[20] The aspect ratio, $\alpha = D/W$, is fixed to 1.

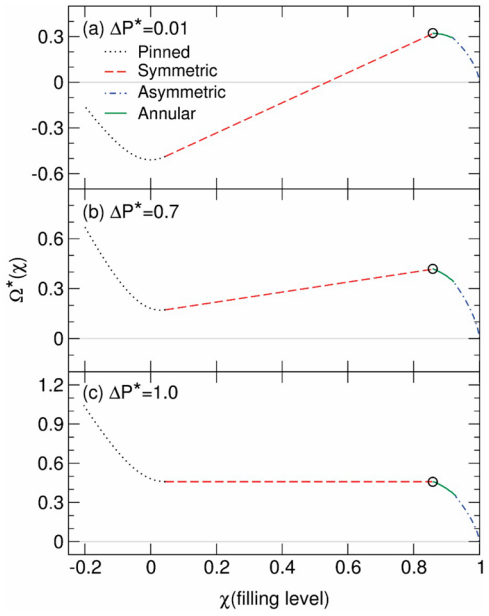

Figure 2. Free-energy profile for the wetting or dewetting transition of a cylindrical cavity. The dimensionless grand potential, Ω*, is plotted vs χ for the cavity with $\theta = 110°$ and $\alpha = 1$. The free energies are calculated for ΔP^*s of 0.01 (a), 0.7 (b), and 1 (c). The Ω*s of the symmetric pinned, symmetric depinned, annular, and asymmetric depinned interfaces are drawn.

Regardless of the pressure, Ω* has a local or global minimum at χ slightly larger than 0 (CB state) and at $\chi = 1$ (WZ state). Note Ω* is always 0 at $\chi = 1$ by construction. For a negative or near 0 value of χ, the liquid–vapor interface is pinned symmetrically (drawn as dotted lines in Figure 1a). As χ increases from 0, the initially pinned interface becomes depinned (broken lines, Figure 1a), and Ω* increases. At a high filling level, $\chi > 0.8$, Ω* culminates at a transition state, marked with the circle in Figure 2. This occurs when the symmetric depinned interface touches the bottom of the cavity and flips its downward curvature to an upward one. The resulting annular interface (drawn as solid lines in Figure 1a) is found for the range, $\chi \sim 0.85$–0.9. With further wetting of the cavity ($\chi > 0.9$), the annular interface becomes asymmetric (drawn as dot-dashed lines), until the liquid–vapor interface disappears and the cavity is fully wetted ($\chi = 1$).

In summary, the wetting transition of a cylindrical cavity begins with an axis-symmetric pinned interface of the liquid and vapor and then proceeds with a symmetric depinned interface and later with an annular interface, finally followed by an asymmetric depinned interface.[21] In contrast, the wetting transition of a rectangular groove has no analogue of the present annular interface. Therefore, it consists of three consecutive steps: a symmetric pinned interface that becomes a symmetric depinned interface followed by an asymmetric depinned interface (see Figure S2 in the Supporting Information).

Note that the relative stabilities of the CB ($\chi \sim 0$) and WZ ($\chi = 1$) states depend on the pressure. At the lowest pressure, $\Delta P^* = 0.01$, the CB state is stable, and the WZ state is metastable (Figure 2a). The free-energy barrier, Ω_B^*, of the wetting (CB-to-WZ) transition is much larger (by 0.51) than that of the dewetting (WZ-to-CB) transition. As ΔP^* increases to 0.7 (Figure 2b), the dewetting transition has a larger free-energy barrier (by 0.17) than that of the wetting transition. Consequently, the CB state becomes metastable, whereas the WZ state becomes stable. A significant barrier still exists for the

DOI: 10.1021/acs.jpcc.7b09757
J. Phys. Chem. C 2018, 122, 2122–2126

transition from the metastable CB state to the WZ state. At the maximum pressure (Figure 2c), $\Delta P^* = 1$, the wetting transition requires no free-energy barrier. Therefore, the WZ state becomes the only stable state.

The annular interface can be unstable, relative to the asymmetric interface, for a less hydrophobic cavity. Using a marginally hydrophobic contact angle, $\theta = 95°$, and a high aspect ratio, $\alpha = 10$, the free-energy profiles for three different pressures is calculated, as shown in Figure 3. The free-energy profiles show

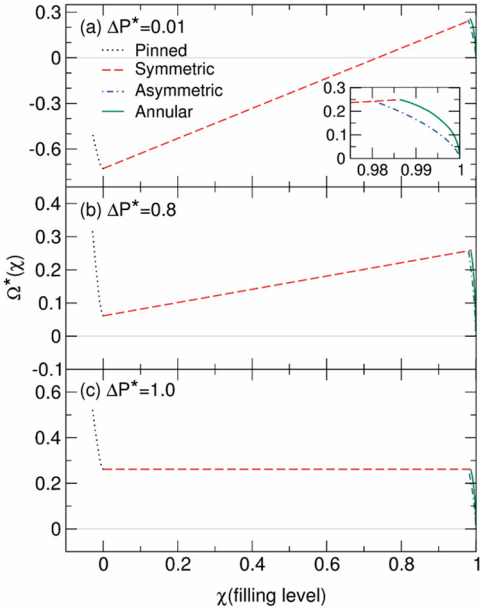

Figure 3. Free-energy profile for the wetting transition of a cylindrical cavity with $\theta = 95°$ and $\alpha = 10$. Ω^* plotted vs χ for ΔP^*s of 0.01 (a), 0.8 (b), and 1 (c). The Ω^*s of the symmetric pinned, symmetric depinned, and asymmetric depinned interfaces are drawn. The Ω^* of the unstable annular interface is shown for comparison (magnified as an inset (a)).

similar tendencies to those found in Figure 2; as ΔP^* increases from 0.01 to 0.8, the CB state becomes metastable, and the WZ state becomes stable. At the maximum pressure, $\Delta P^* = 1$, the free-energy barrier for the wetting disappears, and the WZ state becomes the only stable state. Note that the annular interface is now less stable than the asymmetric interface, regardless of the pressure. The Ω^*s of the annular interfaces (drawn as solid lines) are marginally (by 0.047 at most) higher than those of the asymmetric interfaces (dot-dashed lines). Therefore, the wetting transition in this case proceeds in three, instead of four, steps: an initially symmetrically pinned interface becomes depinned symmetrically and then depinned asymmetrically. This three-step wetting transition is similar to that found for a rectangular groove, even though a cylindrical cavity and a rectangular groove have different symmetries.

Using the free-energy profiles, such as those shown in Figures 2 and 3, the dimensionless free-energy barriers, Ω_B^*s, are calculated for the wetting and dewetting transitions, defined as the differences in the Ω^*s of the CB or WZ state and the transition state, respectively. In Figure 4 (top), Ω_B^* is plotted by continuously varying ΔP^* from 0 to 1. As expected, Ω_B^* for the wetting transition decreases with increasing ΔP^*, and Ω_B^* for the dewetting transition increases with increasing ΔP^*. At the intersection of the Ω_B^* lines of the wetting (dot-dashed line) and dewetting (solid line) transitions (drawn as a circle), the free-energy barriers for the wetting and dewetting transitions become

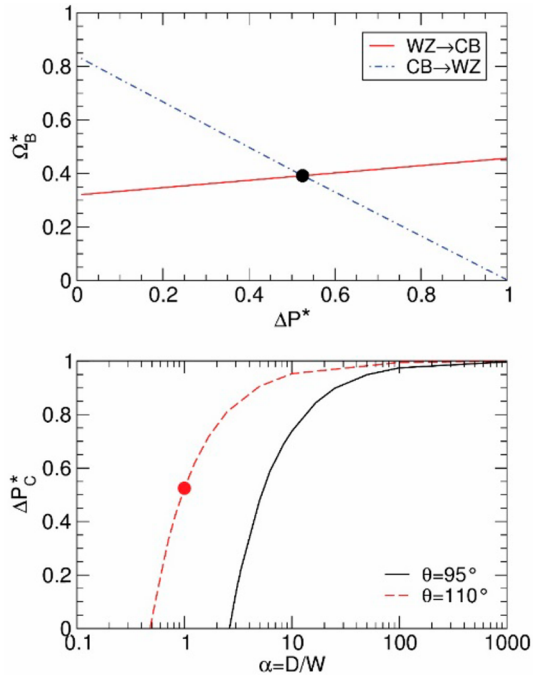

Figure 4. (Top) Dimensionless free-energy barrier Ω_B^* vs the pressure, ΔP^*, for the same θ and α used in Figure 2. The Ω_B^* for the WZ-to-CB transition is plotted vs ΔP^* as a solid line, and Ω_B^* for the CB-to-WZ transition is plotted vs ΔP^* as a dot-dashed line. The intersection of these two lines (drawn as a circle) gives the coexistence pressure, ΔP_C^*, where the CB and WZ states have equal grand potentials (equal stabilities). (Bottom) Coexistence pressure, ΔP_C^*, vs the aspect ratio, α. Note that α is plotted in the log scale. The results for θs of 95° and 110° are drawn as broken and solid lines, respectively. The circle represents the ΔP_C^* shown in the top panel.

identical, meaning that the CB and WZ states are equally stable. This particular pressure is defined as the *coexistence pressure*, ΔP_C^*. Under the condition drawn in the top of Figure 4 ($\theta = 110°$ and $\alpha = 1$), $\Delta P_C^* = 0.5247$ and $\Omega_B^* = 0.3916$.

Figure 4 (bottom) shows how ΔP_C^* depends on the aspect ratio, α, for two different cylindrical cavities with θs of 95° and 110°. Note the WZ state is stable above the coexistence curves drawn as the solid and broken lines, and the CB state is stable below the coexistence curves. Irrespective of θ, ΔP_C^* increases with increasing α, converging to 1 at very high aspect ratios. This indicates that with increasing aspect ratios, the CB state can be stable at a higher pressure. Note also that the ΔP_C^* becomes 0 below a threshold aspect ratio, α_t (2.63 and 0.48 for $\theta = 95°$ and 110°, respectively). This means that for $\alpha < \alpha_t$, the CB state cannot be stable, regardless of the pressure of the liquid drop. Note also that as the surface becomes more hydrophobic (with θ increasing from 95° to 110°), the coexistence curve is shifted left and up, indicating that the CB state can be sustained for a wider range of pressures and aspect ratios. In other words, the CB state can be stable for a smaller aspect ratio and a higher pressure. The Ω_B^* versus pressure and the coexistence curves shown in Figure 4 are qualitatively similar to those observed for a rectangular groove (Figure S3 of the Supporting Information).

By considering the various shapes of the liquid–vapor interface (including a vapor bubble located on the bottom of cylindrical cavity), we report here the interfaces give a minimal free energy, Ω, for a given filling level, χ. In principle, it is possible, although unlikely, that a new type of liquid–vapor interface, not reported here, is found to be stable.

DOI: 10.1021/acs.jpcc.7b09757
J. Phys. Chem. C 2018, 122, 2122−2126

CONCLUSION

A superhydrophobic surface texturized with nano- or microscale cavities finds extremely wide applications. The theories on the wettability of such a surface have focused conventionally on the cases in which the cavities are wetted completely (WZ state) or dewetted (CB state) by a liquid. The various intermediate states that can exist between the CB and WZ states are much less known. In addition, a liquid drop exists in a thermodynamically stable and metastable state.[11,12] In this vein, a theory capable of addressing the metastable and transition states in the wetting transition is highly desirable. This paper presented a theory for the free-energy change in the continuous wetting of a cylindrical cavity, which is a common motif of cavities engraved on hydrophobic surfaces. A cylindrical cavity was wetted in four steps: Initially, the liquid−vapor interface is axis-symmetric and pinned at the top of the cavity. The interface then becomes depinned and slides down along the side wall of the cavity. Upon touching the bottom of the cavity, the liquid−vapor interface becomes annular by inverting its downward curvature. The interface finally becomes asymmetric before coming in contact with the cavity and disappears, giving the fully wetted WZ state. The free-energy barrier for the wetting and dewetting transitions was investigated by systematically varying the aspect ratio of the cavity and the pressure of the liquid. These findings provide fundamental design principles for cavities in superhydrophobic applications.

ASSOCIATED CONTENT

Supporting Information

The Supporting Information is available free of charge on the ACS Publications website at DOI: 10.1021/acs.jpcc.7b09757.

Detailed derivation of eqs 2 and 3, various liquid−vapor interfaces in the wetting of a two-dimensional rectangular groove, free-energy profiles (Ω^* vs χ curves) for the rectangular groove under three different ΔP^*s, Ω_B^* vs ΔP^* and ΔP_C^* vs α for the rectangular groove with three different intrinsic contact angles, details of the derivation of eqs 4−8 (PDF)

AUTHOR INFORMATION

Corresponding Author

*E-mail: jkjang@pusan.ac.kr.

ORCID

Joonkyung Jang: 0000-0001-9028-0605

Notes

The authors declare no competing financial interest.

ACKNOWLEDGMENTS

This study was supported by National Research Foundation Grants funded by the Korean Government (MSIP, NRF-2014R1A4A1001690 and NRF-2015R1A2A2A01004208). This work was also supported by the National Institute of Supercomputing and Network/Korea Institute of Science and Technology Information with supercomputing resources and technical support (KSC-2016-S1-0014).

REFERENCES

(1) Parker, A. R.; Lawrence, C. R. Water Capture by a Desert Beetle. *Nature* **2001**, *414*, 33−34.

(2) Duan, W.; Xie, A.; Shen, Y.; Wang, X.; Wang, F.; Zhang, Y.; Li, J. Fabrication of Superhydrophobic Cotton Fabrics with UV Protection Based on CeO_2 Particles. *Ind. Eng. Chem. Res.* **2011**, *50*, 4441−4445.

(3) Park, K.-C.; Choi, H. J.; Chang, C.-H.; Cohen, R. E.; McKinley, G. H.; Barbastathis, G. Nanotextured Silica Surfaces with Robust Superhydrophobicity and Omnidirectional Broadband Supertransmissivity. *ACS Nano* **2012**, *6*, 3789−3799.

(4) Blossey, R. Self-Cleaning Surfaces - Virtual Realities. *Nat. Mater.* **2003**, *2*, 301−306.

(5) Salvadori, M. C.; Cattani, M.; Oliveira, M. R. S.; Teixeira, F. S.; Brown, I. G. Design and Fabrication of Superhydrophobic Surfaces Formed of Microcavities. *Appl. Phys. Lett.* **2010**, *96*, 074101.

(6) Zhang, Z.; Matin, M. A.; Ha, M. Y.; Jang, J. Molecular Dynamics Study of the Hydrophilic-to-Hydrophobic Switching in the Wettability of a Gold Surface Corrugated with Spherical Cavities. *Langmuir* **2016**, *32*, 9658−9663.

(7) Yong, X.; Zhang, L. T. Nanoscale Wetting on Groove-Patterned Surfaces. *Langmuir* **2009**, *25*, 5045−5053.

(8) Rathgen, H.; Mugele, F. Microscopic Shape and Contact Angle Measurement at a Superhydrophobic Surface. *Faraday Discuss.* **2010**, *146*, 49−56.

(9) Wenzel, R. N. Resistance of Solid Surfaces to Wetting by Water. *Ind. Eng. Chem.* **1936**, *28*, 988−994.

(10) Cassie, A. B. D.; Baxter, S. Wettability of Porous Surfaces. *Trans. Faraday Soc.* **1944**, *40*, 546−551.

(11) Jung, Y. C.; Bhushan, B. Wetting Transition of Water Droplets on Superhydrophobic Patterned Surfaces. *Scr. Mater.* **2007**, *57*, 1057−1060.

(12) Callies, M.; Quéré, D. On Water Repellency. *Soft Matter* **2005**, *1*, 55−61.

(13) Giacomello, A.; Chinappi, M.; Meloni, S.; Casciola, C. M. Metastable Wetting on Superhydrophobic Surfaces: Continuum and Atomistic Views of the Cassie-Baxter−Wenzel Transition. *Phys. Rev. Lett.* **2012**, *109*, 226102.

(14) Kim, H.; Saha, J. K.; Jang, J. Drying Transition of Water Confined between Hydrophobic Pillars. *J. Phys. Chem. C* **2012**, *116*, 19233−19239.

(15) Kim, H.; Lee, S. I.; Matin, M. A.; Zhang, Z.; Jang, J.; Ha, M. Y.; Jang, J. Monte Carlo Study on the Wetting Behavior of a Surface Texturized with Domed Pillars. *J. Phys. Chem. C* **2014**, *118*, 26070−26079.

(16) Orr, F. M.; Scriven, L. E.; Rivas, A. P. Pendular Rings between Solids: Meniscus Properties and Capillary Force. *J. Fluid Mech.* **1975**, *67*, 723−742.

(17) Melrose, J. C. Model Calculations for Capillary Condensation. *AIChE J.* **1966**, *12*, 986−994.

(18) Oliver, J. F.; Huh, C.; Mason, S. G. Resistance to Spreading of Liquids by Sharp Edges. *J. Colloid Interface Sci.* **1977**, *59*, 568−581.

(19) Patankar, N. A. Consolidation of Hydrophobic Transition Criteria by Using an Approximate Energy Minimization Approach. *Langmuir* **2010**, *26*, 8941−8945.

(20) Zhu, L.; Feng, Y.; Ye, X.; Zhou, Z. Tuning Wettability and Getting Superhydrophobic Surface by Controlling Surface Roughness with Well-Designed Microstructures. *Sens. Actuators, A* **2006**, *130−131*, 595−600.

(21) Lv, P.; Xue, Y.; Liu, H.; Shi, Y.; Xi, P.; Lin, H.; Duan, H. Symmetric and Asymmetric Meniscus Collapse in Wetting Transition on Submerged Structured Surfaces. *Langmuir* **2015**, *31*, 1248−1254.

DOI: 10.1021/acs.jpcc.7b09757
J. Phys. Chem. C 2018, 122, 2122−2126